Revealing the size-dependent d-d excitations of cobalt nanoparticles using soft X-ray spectroscopy

Zhangzhang Cui,[†,‡] Chenlu Xie,[§] Xuefei Feng,[¶] Nigel Becknell,[§] Peidong Yang,[§,‖] Yalin Lu,[†,‡] Xiaofang Zhai,[†,‡] Xiaosong Liu,[¶] Wanli Yang,[#] Yi-De Chuang,[,#] Jinghua Guo[*,#,¥]*

[†]Hefei National Laboratory for Physical Sciences at the Microscale and Department of Materials Science and Engineering, University of Science and Technology of China, Hefei 230026, Anhui, China

[‡]Synergetic Innovation Center of Quantum Information and Quantum Physics, University of Science and Technology of China, Hefei 230026, Anhui, China

[§]Department of Chemistry, University of California, Berkeley, CA 94720, USA

[¶]Shanghai Institute of Microsystem and Information Technology, Chinese Academy of Science, Shanghai, China

[‖]Materials Sciences Division, Lawrence Berkeley National Laboratory, Berkeley, CA 94720, USA

[#]Advanced Light Source, Lawrence Berkeley National Laboratory, Berkeley, CA 94720, USA

[¥]Department of Chemistry and Biochemistry, University of California, Santa Cruz, CA 95064, USA

ABSTRACT: Fischer-Tropsch (FT) synthesis is a key step in the gas-to-liquid technology, which is used to produce the liquid fuels through surface-catalyzed polymerization of carbon monoxide and hydrogen. With prominent activity and selectivity, cobalt-based catalysts are widely used in FT reaction; however, the cobalt nanocatalysts can exhibit intriguing size dependent activity whose origin remains heavily debated. To shed light on this issue, the electronic structures of cobalt nanoparticles with size ranging from 4 nm to 9 nm are studied using soft X-ray absorption (XAS) and resonant inelastic X-ray scattering (RIXS) spectroscopy. The XAS and RIXS results demonstrate a stronger Co-O bond in smaller Co nanoparticles. The RIXS measurements reveal the significant size-dependent d-d excitations, from which we determine that the crystal field energy 10Dq changes from 0.6 eV to 0.9 eV when the particle size is reduced from 9 nm to 4 nm. The finding that larger Co nanoparticles exhibit smaller 10Dq is separately confirmed by simulating the Co L-edge RIXS spectra with atomic multiplet code. Our results reveal the modulation of electronic structures by the size of Co nanoparticles, which brings in further insights to their size-dependent catalytic performance.

KEYWORDS: Co nanoparticles, crystal field energy, d-d excitations, X-ray absorption, resonant inelastic X-ray scattering

Cobalt-based catalysts are well known for their prominent activity and selectivity in the Fishcer-Tropsch (FT) synthesis, and their physical and chemical properties have been studied extensively over the past decades.[1,2] One crucial factor that influences the catalytic performance in FT reaction, in particular for Co metal nanocatalysts, is the particle size. It is demonstrated that the reactivity and selectivity of Co nanoparticles towards long-chain hydrocarbon is optimum at the size of ~ 10 nm, but that decreases rapidly when the particle size is below 6 - 8 nm.[3] The origin of this size effect is still heavily debated, despite the tremendous research efforts that have been devoted to this subject thus far. Some studies attributed this size effect to the low reducibility and high re-oxidation tendency of smaller Co nanoparticles, as the metallic Co^0 are the active sites in FT reaction.[4,5] Other studies demonstrated that the dissociation of carbon monoxide (CO) and hydrogen (H_2) is dependent on the size of Co nanoparticles, which leads to variation in the catalytic activity and selectivity.[3,6-8] Additionally, the size-dependent metal surface reconstruction under FT condition was believed to be another relevant factor.[9-11]

An essential prerequisite for gaining further insights to this size effect is the probing of fine electronic structures of Co nanoparticles as a function of particle size. The electronic structures of active Co 3d electrons can be strongly influenced by the local environment around the Co atom. For example, the Co 3d electrons in CoO with octahedral symmetry (O_h) will have $^4T_{1g}(^4F)$, $^4T_{2g}(^4F)$, $^4A_{2g}(^4F)$ multiplet states (Fig. 1(a)), and the energies of these multiplet states set by the geometric configurations and local chemical environment affect the physical and chemical properties of the compound. Although such information may be obtained from fitting the X-ray absorption spectra (XAS) of Co nanoparticles, the core-hole lifetime involved in the XAS

process broadens the spectral lineshape, which limits the precise determination of energetics of multiplet states.

Resonant inelastic X-ray scattering (RIXS) spectroscopy has been extensively used to probe the d-d transitions between these multiplet states in correlated materials. RIXS is a second-order optical process that involves the excitation of electrons from core levels to the unoccupied states (photon absorption) followed by the de-excitation of other electrons in the occupied states back to the core levels (photon emission).[12-14] The energy resolution of RIXS, because of the superposition of photon absorption and emission processes, is not limited by the core-hole lifetime.[15] Depending on the symmetry of ground, intermediate and final states (see Figure 1(a)), the intensity and energy (or energy loss relative to the elastic line) of RIXS features enable the direct measurement of multiplet states of 3d electrons of Co nanoparticles.

In this study, we have performed the systematic investigations of fine electronic structures of Co nanoparticles as a function of particle size using XAS and RIXS at both Co M- and L-edges. Our XAS and RIXS results show that the surface Co atoms in smaller nanoparticles are more susceptible to oxidation. Furthermore, the RIXS measurements clearly reveal the significant size-dependent d-d excitations and reduced crystal field splitting energy 10Dq in larger Co nanoparticles. These results are further confirmed by simulating the L-edge RIXS spectra with atomic multiplet code. Our results suggest the strong modulation of electronic structures by the Co nanoparticle size, which we propose can provide novel insight to their size-dependent catalytic performance.

The transmission electron microscopy (TEM) images of 4, 7 and 9 nm Co nanoparticles are shown in Figure 1(b-d). All TEM images display narrow size distributions, confirming the precise nanoparticle size-control by the heating temperature in the fabrication process. The Co L-

edge XAS of these nanoparticles recorded in TEY (blue) and TFY (red) modes are shown in Figure 1(e), together with the reference spectra of CoO and Co metal samples (black). The XAS spectra in TFY mode exhibit higher $L_2/(L_2 + L_3)$ branching ratio than that of TEY mode, which is due to the saturation effect in the fluorescence detection method.[16] Two groups of manifolds located around 778 eV and 793 eV are related to the spin-orbit splitted Co 2p core levels (Co L_3 and L_2 edges, respectively).[17,18] All three samples show a main peak at 777.5 eV (L_3 edge) and two weak shoulders at 776 eV and 778.5 eV. Compared with the reference spectra, these shoulders can be assigned to the contribution from oxide phase such as CoO, indicating that the surfaces of these nanoparticles are oxidized. The shoulder features become stronger as particle size decreases, suggesting that the smaller nanoparticles are easier to be oxidized.

It is noticed that there are two strong satellite peaks at ~ 6 eV above the main Co L_3/L_2 absorption edges only in the TFY mode of XAS from 9 nm nanoparticles. Similar satellite peaks were reported previously and attributed to the metal-to-ligands charge transfer (MLCT) from the hybridization between transition metal $4p^*/3d$ and ligand π^* orbitals.[16,19-21] In this regard, the satellite peaks seen in Figure 1(e) may come from the charge transfer between Co metal and ligands such as oleic acid. When the surfaces of smaller nanoparticles are oxidized to a much higher degree, this MLCT effect is significantly suppressed beyond detection.

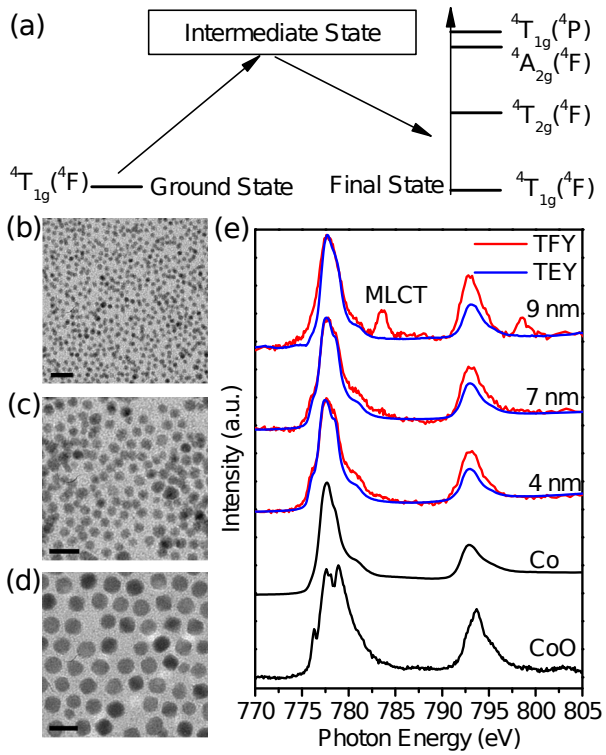

Figure 1. (a) Schematic illustration of RIXS process in CoO with O_h symmetry, where transition takes place from ground state $^4T_{1g}(^4F)$ to intermediate and to $^4T_{1g}(^4F)$ (elastic line), $^4T_{2g}(^4F)$, $^4A_{2g}(^4F)$ and $^4T_{1g}(^4P)$ final states. TEM images of (b) 4 nm, (c) 7 nm and (d) 9 nm Co nanoparticles. The horizontal bar in these images denotes the 20 nm length scale. (e) Normalized XAS spectra of 4, 7 and 9 nm Co nanoparticles recorded in TEY (blue) and TFY (red) modes, together with the reference spectra of CoO and Co metal samples (black).

Figure 2 shows the M-edge XAS and RIXS spectra of 4, 7 and 9 nm Co nanoparticles. The M-edge XAS spectrum of 4 nm nanoparticles recorded in TEY mode is shown in Figure 2(a). In this spectrum, the prominent peak around 61 eV corresponds to the Co M_3 absorption peak. Its energy position, as well as the pre-edge feature around 59.5 eV that resembles the one in the XAS of CoO,[22] suggest that the surface of 4 nm Co nanoparticles is oxidized. This aspect can be further examined by looking at the RIXS spectra shown in Figure 2(b-e). Due to shallower 3p

core holes with extended wave functions that hybridize more strongly with the active occupied 3d orbitals, the transition metal M-edge RIXS spectra are often dominated by the strong elastic peak (zero energy loss) with extended tail, on top of which the RIXS features reside (see Figure 2(b)). Therefore, to highlight the weak RIXS features in this figure, the elastic peak tail is modeled with a polynomial and removed in panels (c) and (d).

Three features denoted P_1, P_2 and P_3 (indicated by the dashed lines) can be seen in the RIXS spectra of 4 nm (Figure 2(c)) and 7 nm (Figure 2(d)) nanoparticles. Their intensities show strong resonance behavior when the incident photon energy is tuned across Co M_3 edge. These peaks have been previously reported and assigned to the excitations between Co 3d states (d-d excitations).[23-25] In the RIXS spectra of 4 nm Co nanoparticles, the peak P_1 has an energy loss of 0.93 eV and maximum intensity around 61 eV, consistent with the results from CoO.[22,25] Thus we can attribute these d-d excitations to the presence of insulating oxide phase like CoO. With increasing particle size, P_1 becomes weaker and eventually disappears as in the case of 9 nm nanoparticles (Figure 2(e)). Since the delocalized 3p core holes can easily decay into the conduction bands in the metallic samples, leading to the suppression of RIXS signal, the intensity evolution of these d-d excitations implies that the metallicity increases with particle size. Besides this intensity behavior, we also notice that the energy position of P_1 is changing with particle size: in 7 nm nanoparticles, it is reduced by roughly 0.1 eV. This point will be further discussed.

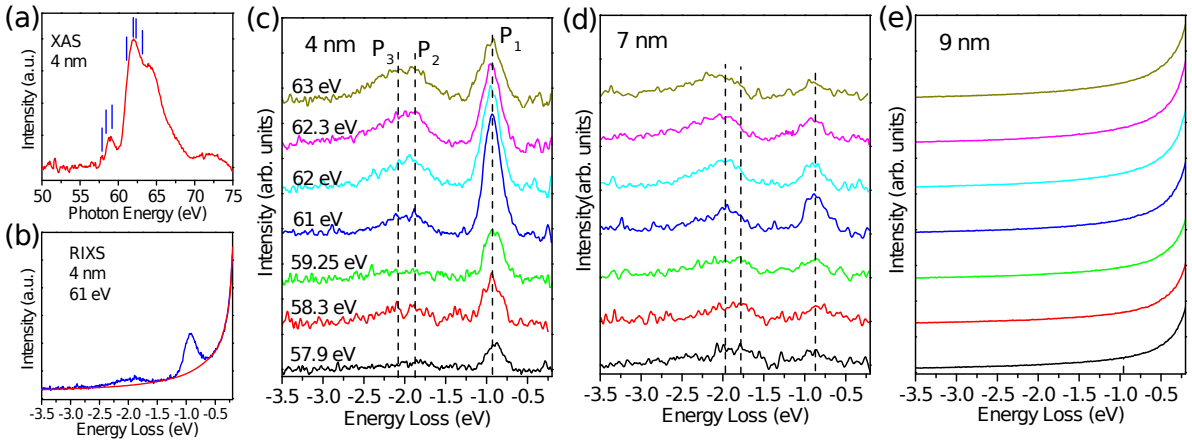

Figure 2. (a) M-edge XAS spectrum of 4 nm Co nanoparticle recorded in TEY mode. (b) M-edge RIXS spectrum of 4 nm Co nanoparticles at 61 eV. The red line marks the polynomial fit to the elastic tail. M-edge RIXS spectra of (c) 4 nm (elastic tail subtracted), (d) 7 nm (elastic tail subtracted) and (e) 9 nm Co nanoparticles. The incident photon energy is displayed in the RIXS spectra of 4 nm nanoparticles (also indicated by vertical lines in panel (a)) and traces with same color to the same incident photon energy. Peaks P_1, P_2 and P_3 are denoted by the dashed lines in panels (c) and (d).

Although the M-edge RIXS spectroscopy gives much better energy resolution to resolve the d-d excitations, the RIXS cross-section is extremely low that prohibits us from studying the fine spectral structures. Therefore, we carried out the Co L-edge RIXS measurements. Figure 3 (a-c) shows the L-edge RIXS maps (RIXS intensity displayed as a function of incident and emission photon energies) of 4, 7 and 9 nm Co nanoparticles. There are three main features in these RIXS maps: the strong diagonal line towards the bottom right part of the maps, the corresponding "parallel" diagonal lines and vertical stripes around 776 eV and 792 eV emission energies. The strong diagonal line is the elastic line where the emission photon energy is the same as the incident photon energy (zero energy loss). The weaker diagonal lines parallel to the elastic line

are the excitations with fixed energy loss. In this case, they are the Co 3d d-d and charge-transfer excitations. The vertical stripes are features with constant emission energies, and they are known to be the $L_{2,3}$ normal emissions from valence band transitions. In all RIXS maps, strong resonance effects are observed at both Co L_3 and L_2 thresholds, suggesting that the aforementioned features are intrinsic to the Co nanoparticles under study and not the experimental artifacts. We notice that the relative intensity of L_3 normal emissions (vertical stripe at 776 eV) to L_2/L_3 RIXS features increase dramatically with increasing particle size. Since the RIXS channel in bulk cobalt metal is suppressed by the competing Auger channel due to the enhanced decay of core holes in the intermediate state, which can also lead to much stronger L_3 normal emissions, this intensity ratio offers the direct measure of surface oxide phase relative to the interior Co metal phase. As particle size increases, the evolution of this intensity ratio signifies that the fraction of surface Co oxide is reduced, consistent with the results from XAS and M-edge RIXS presented earlier.

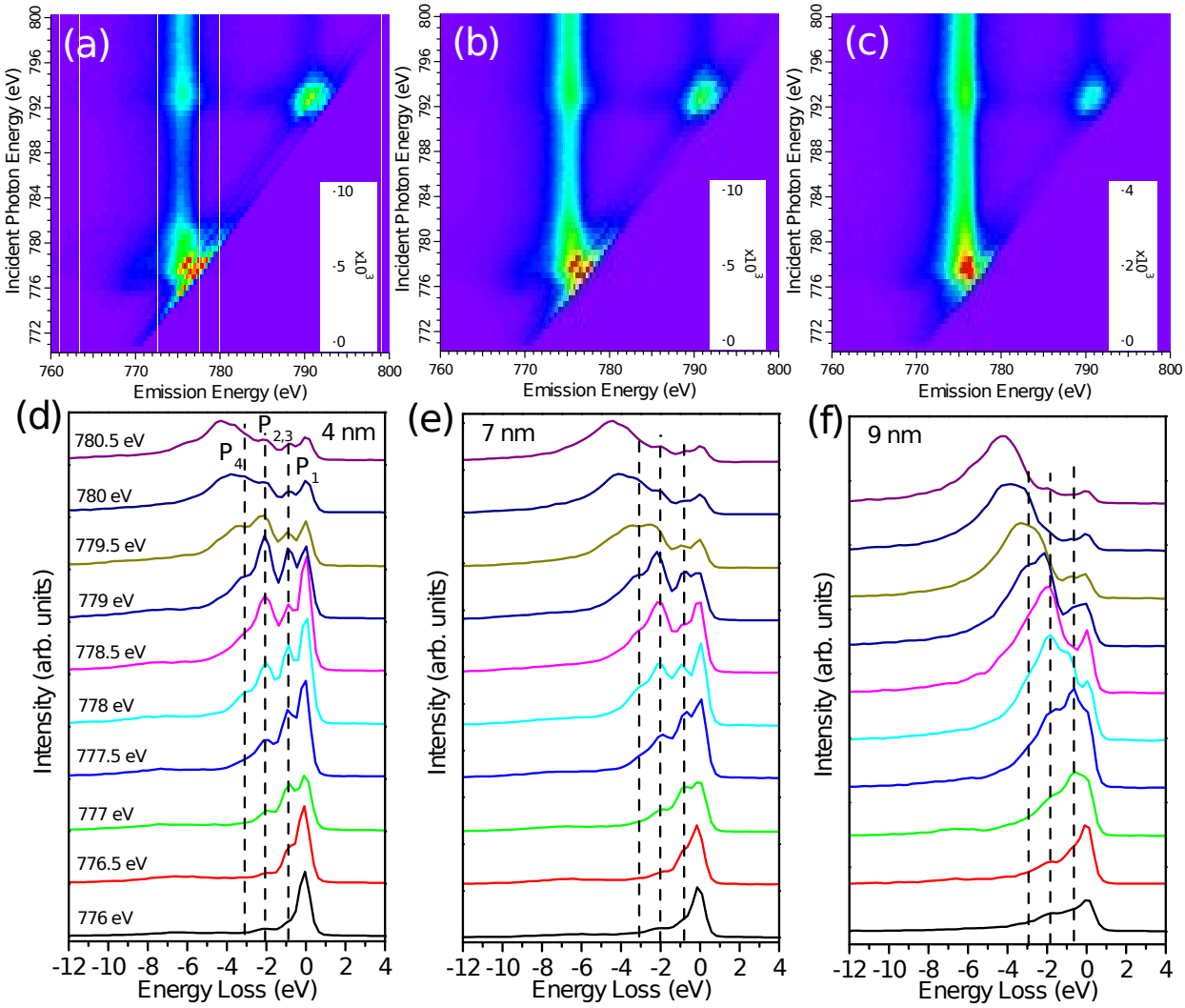

Figure 3. Co L-edge RIXS maps of (a) 4 nm, (b) 7 nm and (c) 9 nm Co nanoparticles. The incident photon energy step is 0.5 eV. (d-f) Detailed L-edge RIXS spectra at the Co L_3 threshold of (d) 4 nm, (e) 7 nm and (f) 9 nm Co nanoparticles with the same incident photon energies plotted on an energy loss scale. The spectra were extracted from the RIXS maps in panels (a-c). The incident photon energies are displayed in the RIXS spectra of 4 nm nanoparticles. The curves with same color correspond to the same incident photon energy.

More information can be obtained by looking at the horizontal line cuts (fixed incident photon energies) in these RIXS maps. Figure 3 (d-f) shows the selected L-edge RIXS spectra around the Co L_3 threshold. A broad set of weak peaks around 7 eV energy loss can be attributed to the charge-transfer excitations between Co 3d and O 2p orbitals.[17,20] The pronounced d-d excitation peaks P_1, $P_{2,3}$ and P_4 (indicated by the dashed lines) can be clearly seen in all spectra. The intensity of these d-d excitations exhibits a significant size-dependent behavior, implying noticeable changes in the 3d electronic states of surface Co atoms in these nanoparticles. In addition to the intensity behavior, we also notice that the energies of d-d excitations decrease slightly when the particle size increases, consistent with the M-edge RIXS results shown in Figure 2.

In the case of Co^{2+} under O_h crystal field, the spherical symmetric ^4F ground state splits into $^4T_{1g}(^4F)$, $^4T_{2g}(^4F)$ and $^4A_{2g}(^4F)$ multiplet states (see Figure 1(a)). The first peak P_1 in Figure 3 (d-f) can be assigned to the transition from $^4T_{1g}(^4F)$, the ground state in O_h symmetry, to $^4T_{2g}(^4F)$ multiplet state.[17,26] The second peak $P_{2,3}$ around 2 eV energy loss is the overlap of the transitions from $^4T_{1g}(^4F)$ to $^4A_{2g}(^4F)$ and $^4T_{1g}(^4P)$.[26] The 10Dq value, which is the measure of ligand field strength, can be estimated from the energy difference between $^4T_{1g}(^4F)$ and $^4T_{2g}(^4F)$ or between $^4T_{2g}(^4F)$ and $^4A_{2g}(^4F)$. Although it is proposed that $^4T_{1g}(^4F)$ hybridizes with $^4T_{1g}(^4P)$,[26,27] the 10Dq value derived from the M-edge RIXS spectra with these two methods doesn't show notable deviation, suggesting that the energy difference between $^4T_{1g}(^4F)$ and $^4T_{2g}(^4F)$ can give the reasonable estimation of 10Dq. In that regard, the 10Dq values of 4, 7 and 9 nm Co nanoparticles determined from the energy position of P_1 are ~ 0.9, 0.8 and 0.6 eV, respectively.

To better understand the size-dependent intensity and energy of d-d excitations, as well as the overall lineshape of Co L-edge RIXS spectra, we have performed the crystal field multiplet

simulations for Co^{2+} using the code developed by de Groot et al.[28,29] The calculations simulate the $2p^63d^7 \rightarrow 2p^53d^8 \rightarrow 2p^63d^8\underline{d}$ transitions, where $\underline{d}$ denotes a hole in the Co^{2+} 3d levels. Figure 4 shows the comparison of experimental (black) and simulated (colored) RIXS spectra. Although the experimental RIXS spectra do not exhibit rich structures as the simulated ones, presumably due to much worse energy resolution, the agreement between them is satisfactory considering that there are no other free parameters to tweak in these multiplet calculations and the agreement extends over several incident photon energies. This implies that the multiplet parameters are correctly chosen and the simulations capture the essence of RIXS spectra. The calculations suggest that the size-dependent intensity and lineshape of the RIXS spectra indeed result from the reduced 10Dq as particle size increases.

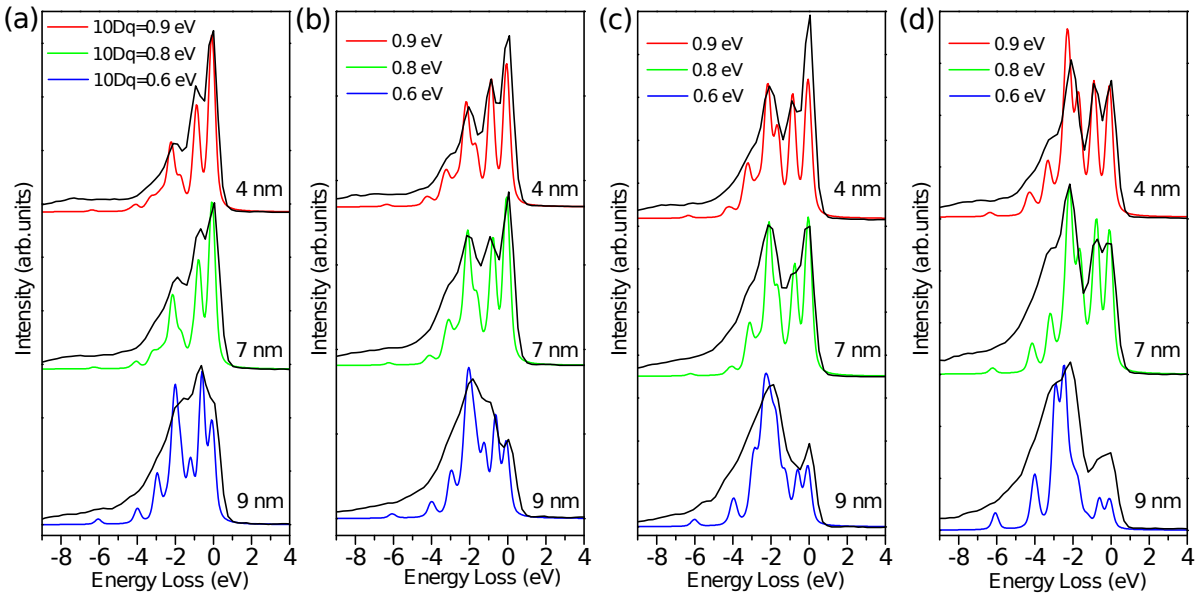

Figure 4. Comparison of simulated (colored) and experimental (black) Co L-edge RIXS spectra of 4 (top), 7 (middle) and 9 nm (bottom) Co nanoparticles at (a) 777.5 eV, (b) 778 eV, (c) 778.5 eV and (d) 779 eV incident photon energy. The intensity of these spectra is rescaled for clarity.

In order to investigate the influence of annealing and reduction process on the electronic structures, the 4 nm Co nanoparticles were further annealed in air and reduced by H_2 to remove the ligands. The TEM image in Figure 5(a) shows that after these treatments, most nanoparticles retain their original size, except some sintered together. The XAS spectra (Figure 5(b)) indicate that the nanoparticles mainly consist of Co metal. Interestingly, we can see that the MLCT peaks similar to the ones seen in the 9 nm as-grown nanoparticles start to show up. This implies that the treated 4 nm nanoparticles behavior more similar to larger untreated nanoparticles. The RIXS spectra of treated nanoparticles at selected photon energies are shown Figure 5(c), overlaid with multiplet simulations (black curve). It is found that to reach a better agreement between them, the 10Dq value needs to be reduced from 0.9 eV to 0.7 eV. This suggests that the electronic structures of nanoparticles were changed during the annealing and reduction process. One possibility is that the reduced 10Dq is the outcome of size increase as seen in the TEM images, and this conjecture is in line with the RIXS results of the as-prepared Co nanoparticles. Another possibility is that it is intrinsic to the Co nanoparticles where surface Co atoms are modified to be more resilient to oxidation.

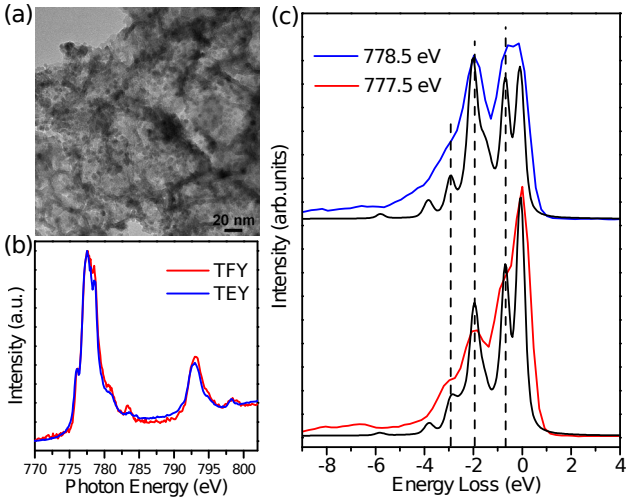

Figure 5. (a) TEM image (Scale bar: 20 nm), (b) XAS and (c) RIXS spectra of 4 nm Co nanoparticles after annealing and reduction treatments. In the RIXS panel, the color curve is the experimental spectra and the black curve is the simulated results.

The significant size-dependent d-d excitations and crystal field splitting energy 10Dq of Co nanoparticles signify the strong modulation on the electronic structures by particle size. The reduced 10Dq in larger Co nanoparticles indicates weaker interactions between Co and O atoms, or equivalently, the weaker Co-O bond. This weaker Co-O bond is in agreement with the finding that larger Co nanoparticles are more resilient to oxidation. It is reported that the Co-O bond forms during the CO dissociation on the surface of Co nanoparticles in FT reaction;[3,30] thus, the variation of Co-O bond strength with size may be a relevant factor in the size-dependent catalytic performance of Co nanoparticles.

In summary, the electronic structures of 4, 7 and 9 nm Co nanoparticles are studied using XAS and RIXS spectroscopies at Co M- and L-edges. Both XAS and RIXS results suggest the decrease of Co-O bond strength with increased Co nanoparticle size. Furthermore, our RIXS results clearly reveal the significant size-dependent d-d excitations. The crystal field splitting energy 10Dq in the 4, 7 and 9 nm Co nanoparticles are determined to be ~ 0.9, 0.8 and 0.6 eV, respectively. The evolution of the intensity of the d-d excitations and the reduction of 10 Dq in larger Co nanoparticles were confirmed from the multiplet simulations of Co^{2+}. These findings signify the modulation of electronic structures of Co nanoparticles as a function of particle size, which bring in new insights to the size-dependent catalytic performance of Co nanoparticles.

Methods. *Sample Preparation.* Mono-dispersed Co nanoparticles with sizes of 4, 7 and 9 nm were synthesized by decomposing the carbonyl precursor $Co_2(CO)_8$ in o-dichlorobenzene in

presence of oleic acid at 180 °C, 172 °C and 168 °C, respectively. The size of nanoparticles was precisely controlled by the heating temperature and determined by the transmission electron microscopy (TEM). The liquid suspended nanoparticles were dropped onto silicon wafers in the glove box under nitrogen atmosphere. From these as-grown samples, the 4 nm Co nanoparticles were further chosen to be loaded onto mesoporous silica support (MCF-17), annealed at 350 °C in air for 1 hour to remove the ligands and then reduced at 350 °C in H_2/Ar (10% H_2) for 2 hours. All samples were transferred to the experimental chambers using portable vacuum suitcase to avoid oxidation and/or contamination.

XAS and RIXS Measurements. The M- and L-edge XAS/RIXS measurements were performed at beamlines 4.0.3 and 8.0.1 at the Advanced Light Source (ALS), Lawrence Berkeley National Laboratory (LBNL). All spectra were recorded at room temperature. The XAS spectra were recorded in both total electron yield (TEY, sample-to-ground drain current) and total fluorescence yield (TFY) modes, and normalized by the incident photon flux determined from the photocurrent of an upstream Au mesh. For RIXS measurements, the incident photon polarization was linear in the horizontal scattering plane (π-polarization). The scattered photons from samples were recorded by x-ray spectrometers at 90° angle relative to the incident photon beam. The combined energy resolution for M-edge and L-edge RIXS determined from the full width half maximum (FWHM) of elastic peak are about 0.025 eV and 0.5 eV, respectively.

Multiplet Calculation. The Co L-edge RIXS spectra are simulated using the code developed by de Groot et al. For simplicity, we do not include the charge-transfer effect. The Coulomb repulsion, exchange interaction and 3d spin-orbit interaction are reduced to 64%, 64% and 80% of the Hartree-Fock values, respectively. The experimental scattering geometry is adopted in the

simulation. The octahedral symmetry is used and the crystal field splitting parameter 10Dq is set to the experimental values: 0.9, 0.8 and 0.6 eV for 4, 7 and 9 nm nanoparticles.

ASSOCIATED CONTENT

Supporting Information.

Detailed sample preparation procedure; TEM images, L-edge XAS/RIXS of 4 and 7 nm Co nanoparticles after annealing and reduction treatments.

AUTHOR INFORMATION

Corresponding Author

*E-mail: ychuang@lbl.gov (Y.-D.C), jguo@lbl.gov (J.-H.G.)

Notes

The authors declare no competing financial interest.

Author Contributions

The manuscript was written through contributions of all authors. All authors have given approval to the final version of the manuscript.

ACKNOWLEDGMENT

The Advanced Light Source is supported by the Director, Office of Science, Office of Basic Energy Sciences, of the U.S. Department of Energy under Contract No. DE-AC02-05CH11231.

REFERENCES

(1) Khodakov, A. Y.; Chu, W.; Fongarland, P. *Chem. Rev.* **2007**, *107*, 1692.

(2) Iglesia, E. *Appl. Catal., A* **1997**, *161*, 59.

(3) Tuxen, A.; Carenco, S.; Chintapalli, M.; Chuang, C. H.; Escudero, C.; Pach, E.; Jiang, P.; Borondics, F.; Beberwyck, B.; Alivisatos, A. P.; Thornton, G.; Pong, W. F.; Guo, J. H.; Perez, R.; Besenbacher, F.; Salmeron, M. *J. Am. Chem. Soc.* **2013**, *135*, 2273.

(4) Jacobs, G.; Das, T. K.; Zhang, Y. Q.; Li, J. L.; Racoillet, G.; Davis, B. H. *Appl. Catal., A* **2002**, *233*, 263.

(5) Schanke, D.; Hilmen, A. M.; Bergene, E.; Kinnari, K.; Rytter, E.; Adnanes, E.; Holmen, A. *Energy Fuels* **1996**, *10*, 867.

(6) den Breejen, J. P.; Radstake, P. B.; Bezemer, G. L.; Bitter, J. H.; Froseth, V.; Holmen, A.; de Jong, K. P. *J. Am. Chem. Soc.* **2009**, *131*, 7197.

(7) Yang, J.; Tveten, E. Z.; Chen, D.; Holmen, A. *Langmuir* **2010**, *26*, 16558.

(8) Herranz, T.; Deng, X.; Cabot, A.; Guo, J.; Salmeron, M. *J. Phys. Chem. B* **2009**, *113*, 10721.

(9) Bezemer, G. L.; Bitter, J. H.; Kuipers, H.; Oosterbeek, H.; Holewijn, J. E.; Xu, X. D.; Kapteijn, F.; van Dillen, A. J.; de Jong, K. P. *J. Am. Chem. Soc.* **2006**, *128*, 3956.

(10) Geerlings, J. J. C.; Zonnevylle, M. C.; Degroot, C. P. M. *Surf. Sci.* **1991**, *241*, 315.

(11) Prieto, G.; Martinez, A.; Concepcion, P.; Moreno-Tost, R. *J. Catal.* **2009**, *266*, 129.

(12) Kotani, A.; Shin, S. *Rev. Mod. Phys.* **2001**, *73*, 203.

(13) Hatton, P. D.; Wilkins, S. B.; Beale, T. A. W.; Johal, T. K.; Prabhakaran, D.; Boothroyd, A. T. *J. Magn. Magn. Mater.* **2005**, *290-291*, 891.

(14) Ament, L. J. P.; van Veenendaal, M.; Devereaux, T. P.; Hill, J. P.; van den Brink, J. *Rev. Mod. Phys.* **2011**, *83*, 705.

(15) Yi, L.; Agren, H.; Gelmukhanov, F.; Guo, J. H.; Skytt, P.; Wassdahl, N.; Nordgren, J. *Phys. Rev. B* **1995**, *52*, 14479.

(16) Hongjian, L.; Jinghua, G.; Yadong, Y.; Augustsson, A.; Chungli, D.; Nordgren, J.; Chinglin, C.; Alivisatos, P.; Thornton, G.; Ogletree, D. F.; Requejo, F. G.; de Groot, F.; Salmeron, M. *Nano Lett.* **2007**, *7*, 1919.

(17) Magnuson, M.; Butorin, S. M.; Guo, J. H.; Nordgren, J. *Phys. Rev. B* **2002**, *65*.

(18) Yoon, W.-S.; Kim, K.-B. *J. Phys. Chem. B* **2002**, *106*, 2526.

(19) Hatsui, T.; Takata, Y.; Kosugi, N. *Chem. Phys. Lett.* **1998**, *284*, 320.

(20) Hatsui, T.; Takata, Y.; Kosugi, N. *J. Synchrotron Radiat.* **1999**, *6*, 376.

(21) Moulin, C. C. D.; Villain, F.; Bleuzen, A.; Arrio, M. A.; Sainctavit, P.; Lomenech, C.; Escax, V.; Baudelet, F.; Dartyge, E.; Gallet, J. J.; Verdaguer, M. *J. Am. Chem. Soc.* **2000**, *122*, 6653.

(22) Wray, L. A.; Li, J.; Qiu, Z. Q.; Wen, J.; Xu, Z.; Gu, G.; Huang, S.-W.; Arenholz, E.; Yang, W.; Hussain, Z.; Chuang, Y.-D. *Phys. Rev. B* **2013**, *88*.

(23) Augustsson, A.; Henningsson, A.; Butorin, S. M.; Siegbahn, H.; Nordgren, J.; Guo, J. H. *J. Chem. Phys.* **2003**, *119*, 3983.

(24) Schmitt, T.; Duda, L. C.; Matsubara, M.; Augustsson, A.; Trif, F.; Guo, J. H.; Gridneva, L.; Uozumi, T.; Kotani, A.; Nordgren, J. *J. Alloys Compd.* **2004**, *362*, 143.

(25) Chiuzbăian, S. G.; Schmitt, T.; Matsubara, M.; Kotani, A.; Ghiringhelli, G.; Dallera, C.; Tagliaferri, A.; Braicovich, L.; Scagnoli, V.; Brookes, N. B.; Staub, U.; Patthey, L. *Phys. Rev. B* **2008**, *78*.

(26) van Schooneveld, M. M.; Kurian, R.; Juhin, A.; Zhou, K.; Schlappa, J.; Strocov, V. N.; Schmitt, T.; de Groot, F. M. F. *J. Phys. Chem. C* **2012**, *116*, 15218.

(27) Tanabe, Y.; Sugano, S. *J Phys Soc Jpn* **1954**, *9*, 753.

(28) Groot, F. d. *Coord. Chem. Rev.* **2005**, *249*, 31.

(29) Bazin, D.; Kovács, I.; Guczi, L.; Parent, P.; Laffon, C.; De Groot, F.; Ducreux, O.; Lynch, J. *J. Catal.* **2000**, *189*, 456.

(30) Shetty, S.; van Santen, R. A. *Catal. Today* **2011**, *171*, 168.